Chapter 4

Structural, optical, dielectric, magnetic and magnetoelectric properties of Co-doped ZnO nanoparticles

4.1. Introduction:

The potentiality of manipulating both the degrees of freedom for charge and spin in DMS empowers these materials to apply in spintronics in which carrier spins are capable to transport, accumulate and process information [223, 224]. The mutual monitor of these degrees of freedom is the basis of these devices with interesting functionalities and enhanced activities. TM modified wide band gap semiconductors have potentiality to fulfill the criterion of DMS. ZnO, wide band gap semiconductor (3.37 eV) possesses high solubility for doping of TM ions and is a promising material for DMS. Room temperature ferromagnetism in the DMS is an important criterion for application in spintronic and electromagnetic coupling devices. Recently researchers perceived that TM (Co, Ni, Fe, V and Mn) doped ZnO [33, 193, 225, 226] explore room temperature ferromagnetic behaviors which have created a growing interest in transition metal modified ZnO DMS. The magnetic properties of the DMS are expected to be controlled by the magnetic moment and density of the dopant ions. In the previous chapter we have examined the material properties of nickel doped ZnO for such applications. The reported magnetic moment of the transition metal ion Co^{2+} is $4.8\mu_B$ is quite higher to that of Ni^{2+} which stands at $2.9\mu_B$. Further, the ionic radius of Co^{2+} ion is nearly equal to that of Zn^{2+} and thus Co^{2+} ion has the highest probability of being adaptable to ZnO host crystal. These observations point to better DMS properties in Co-doped ZnO than that in Ni-doped ZnO samples. In continuation of our investigation on transition metal doped ZnO, here we report our investigations on $Zn_{1-x}Co_xO$ nanoparticles.

Though several articles in different journals have reported on ferromagnetic properties at room temperature in TM doped ZnO since the year 2000 [110, 111, 114], none of the literature have conveyed on the ME coupling effect of these compounds. The ME coupling is the basis of controlling two degrees of freedom in the DMS. We here report the synthesis of $Zn_{1-x}Co_xO$ (x = 0, 0.06, 0.12, 0.18) nanoparticles using a simple and inexpensive chemical

precipitation process and the optical, dielectric, magnetic and ME coupling properties of the prepared samples. The nanoparticles have been characterized by XRD, TEM, FTIR, UV-Vis absorption, FL, dielectric, SQUID and ME coupling measurements.

4.2. Experimental details:

The $Zn_{1-x}Co_xO$ (x = 0, 0.06, 0.12, 0.18) nanopowders were synthesized through chemical precipitation technique by taking cobalt acetate tetrahydrate [$Co(CH_3CO_2)_2 \cdot 4H_2O$; ≥98% Sigma Aldrich] and zinc acetate dihydrate (≥98% Sigma Aldrich) as the starting materials and oxalic acid (≥99.5% Sigma Aldrich) as precipitating reagent. Deionized water was used as solvent to prepare aqueous solutions of oxalic acid (0.5 M) and acetates (0.5 M). Doping concentration x depends on the stoichiometry of the precursors' concentration. For the synthesis of $Zn_{1-x}Co_xO$ for various values of x, we have added 60*(1-x) ml zinc acetate solution, 60* x ml of cobalt acetate solution and 60 ml oxalic acid solution and then mixed up by vigorous stirring using magnetic stirrer. Requisite amount of ammonium hydroxide solution (25% aqueous NH_4OH) was added to retain the pH at 8 ± 0.2. Tetraethylammonium hydroxide [25% $(C_2H_5)_4N(OH)$] was used to avoid agglomeration. The precipitation was conceded at room temperature under constant stirring condition. Stirring process was continued for 2 hour to yield completely reacted nanoparticles with nanosized grain distribution. The temperature and the time are set in such a way as to maintain a higher reaction rate and allowing the reaction to achieve completion respectively. The post-precipitation phases were aged by 24 hour. The precipitates were collected by centrifugation at 6500 rpm for 5 minutes and the process was continued 5 times for each sample. The collected precipitates were dried at 150 ^oC and annealed at 500 ^oC for 2 hour for better stability. The annealed compounds were compacted into pellets for dielectric characterization.

XRD, TEM, HRTEM, FTIR, UV-Vis absorption, FL, dielectric, SQUID and ME coupling characterizations of the $Zn_{1-x}Co_xO$ nanoparticles have been studied.

4.3. Results and discussions:

4.3.1. XRD characterization:

The X-ray diffraction patterns of the nanopowders for different doping concentrations are displayed in figure 4.1. XRD characterization of all the samples approve the hexagonal wurtzite crystal structure with space group $P6_3mc$ on comparing with the available JCPDS (JCPDS 89-0510) [227] data. The ZnO structure is comprised of two interpenetrating hexagonal close packed structures of Zn^{2+} and O^{2-} ions displaced along c-axis. The highest intensity diffraction peak corresponds to the diffraction from (101) plane. The very weak diffraction peaks at 44.83^o, 59.24^o and 65.06^o in the XRD pattern of the compounds indicate the presence of a secondary phase of Co_3O_4. The peak intensity related to secondary phase increases with increasing cobalt concentration [119]. The average crystallite size of the pure and doped nanoparticles were calculated according to Debye-Scherrer equation

$$D = \frac{k\lambda}{\beta Cos\theta} \qquad (4.1)$$

Where D = average crystallite size, k = 0.9 (particle shape factor), λ = wavelength of X-ray radiation, β = FWHM and θ being the Bragg angle.

The average crystallite size conferring to (100) and (101) peaks of different cobalt concentrations are presented in table-V. It is seen from the table that there is a decrease in crystallite size from 25 nm to 15 nm with increasing cobalt concentration from zero to 18%. The relatively smaller size of cobalt ion (ionic radius 0.58 Å) as compared to Zn (ionic radius of 0.60 Å) [119] in the tetrahedral coordination seems to constrain the crystal growth. The systematic decrement in diffraction peak intensity corresponding to the wurtzite structure in the $Zn_{1-x}Co_xO$ compounds is a corollary of the decrement of coherently diffracted domain

size with an endorsement on behalf of replacement of Zn^{2+} ions by Co^{2+} ions. In literature survey it has been conveyed that the maximum incorporation of cobalt in host ZnO is 15% [228-231]. However, the solubility limit of cobalt could be increased to 18% using co-precipitation technique.

Table-V. The average crystallite size of $Zn_{1-x}Co_xO$ series.

Sample	D (nm) of (100) peak	D (nm) of (101) peak
ZnO	25.00	22.6
$Zn_{0.94}Co_{0.06}O$	21.05	20.4
$Zn_{0.88}Co_{0.12}O$	20.19	14.4
$Zn_{0.82}Co_{0.18}O$	15.07	12.6

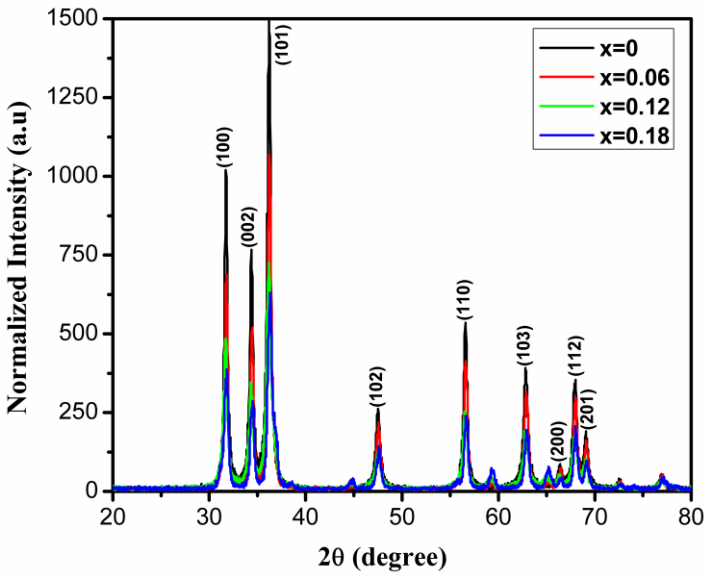

Fig. 4.1. XRD patterns of $Zn_{1-x}Co_xO$ series.

4.3.2. TEM and SAED:

The TEM photograph of $Zn_{0.94}Co_{0.06}O$ nanosample is presented in figure 4.2(a). The surface morphology of the compound is found to be hexagonal with average crystallite size of 30 nm which is nearly same crystallite size calculated from XRD data. From HRTEM photograph (figure 4.2(b)), the interplanar spacing is found to be 0.28 nm. The interplanar distance for the XRD peak at 31.82^o corresponding to the reflection from the (100) planes in the sample amounts to 0.2813 nm. As such, [100] is the favored crystal growth direction in

the sample [194]. The SAED pattern is exhibited in figure 4.3(a). Self-organization and single crystalline nature of the nanoparticles in hexagonal pattern are revealed through SAED pattern. The chemical conformation of the nanosamples is tested by EDX spectroscopy study. The EDX spectra of $Zn_{0.94}Co_{0.06}O$ sample is displayed in figure 4.3(b) which endorse the existence of zinc and cobalt ions in the matrix in conformity with XRD recordings.

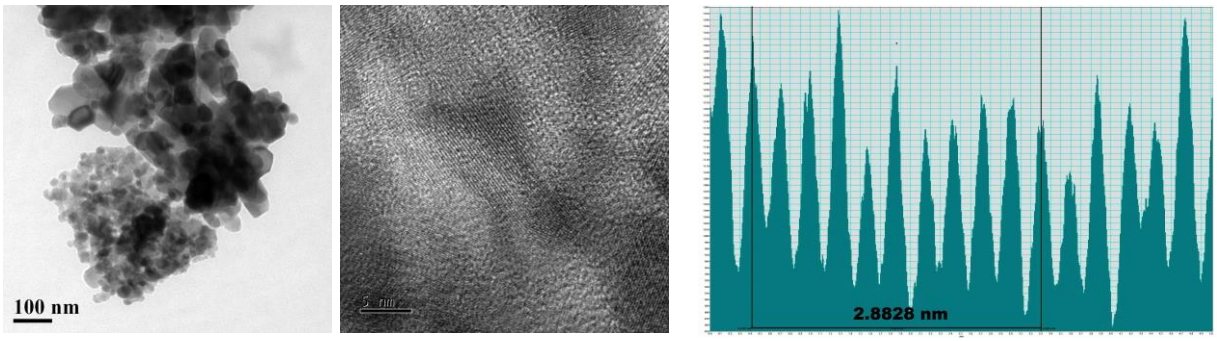

(a) **(b)**

Fig. 4.2. **(a)** TEM image and **(b)** HRTEM photograph of $Zn_{0.94}Co_{0.06}O$ sample.

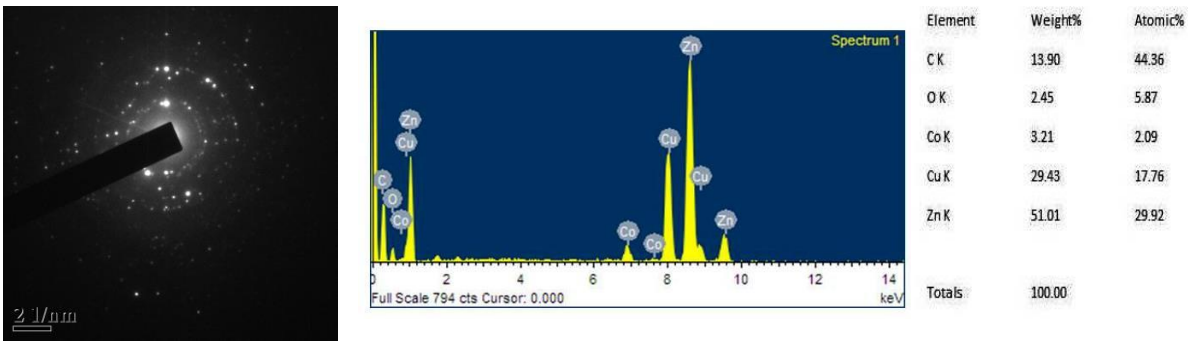

(a) **(b)**

Fig. 4.3. **(a)** SAED pattern and **(b)** EDX spectra of $Zn_{0.94}Co_{0.06}O$ sample.

The EDX spectra do not reveal the percentage of the light element oxygen correctly as the secondary emission of X-ray from the light elements (atomic no less than 10) are soft in nature and gets absorbed. The count lines of C and Cu corresponds to the two electrodes. The atomic ratio of Co to (Zn+Co) in the $Zn_{0.94}Co_{0.06}O$ sample as per the EDX spectra thus amounts to 2.09/ (2.09 + 29.92) = 0.065 which is close to the stoichiometric value of 0.06. Similarly the ratio of Zn to (Zn+Co) in the sample is 29.92/ (2.09+29.92) = 0.935 which is very close to the stoichiometric value of 0.94.

4.3.3. FTIR spectra:

The effect of cobalt doping on structural and vibrational bonds on the hexagonal wurtzite ZnO structure is acquainted from the FTIR spectra. The FTIR spectra of $Zn_{1-x}Co_xO$ nanopowders are presented in figures 4.4(a) and 4.4(b). The absorption peak 424.66 cm^{-1} is originated from stretching mode of Zn–O which approves the formation of wurtzite crystal structure in cobalt doped ZnO nanoparticles. Two characteristic absorption peaks at 602 and 678 cm^{-1} relating to stretching vibration of Co–O–Co and Co–O–Zn have been observed. The relative intensity of these peaks increases with the cobalt concentration except for the sample (x = 0.12). Although, for this sample, the peak positions concur with other Co-doped samples confirming the structural and compositional purity, the decrease in relative intensity of the peaks corresponding to stretching mode of Zn–O, Co–O–Co and Co–O–Zn indicate some distortion that might have caused with the creation of the oxygen vacancy in the sample. An insignificant anomaly at 555 cm^{-1} may be accredited to lattice distortion like oxygen vacancies. While the weak absorption band at 890 cm^{-1} attributes to O–C=O bridging oxalate group, the absorption peaks at 1389 and 1632 cm^{-1} are related to symmetric and asymmetric stretching of the carboxyl group (C=O) [207]. The absorption band at 3434 cm^{-1} corresponds to the O–H stretching of atmospheric water due to hygroscopic nature of ZnO. The peaks at 2800 and 2850 cm^{-1} are attributed to the stretching vibrations of C–H mode.

The three major peaks around 424.66 cm^{-1}, 602 cm^{-1} and 678 cm^{-1} endorse structural evidence and the replacement of the relatively smaller Co^{2+} ions at Zn^{2+} sites of the host ZnO wurtzite structure. The concurrence of the peak at 424.66 cm^{-1} corresponding to stretching vibration of Zn–O in our sample with the widely accepted value of 424 cm^{-1} in bulk ZnO, infers that cobalt doping in the synthesis process did not yield any strain in the lattice structure.

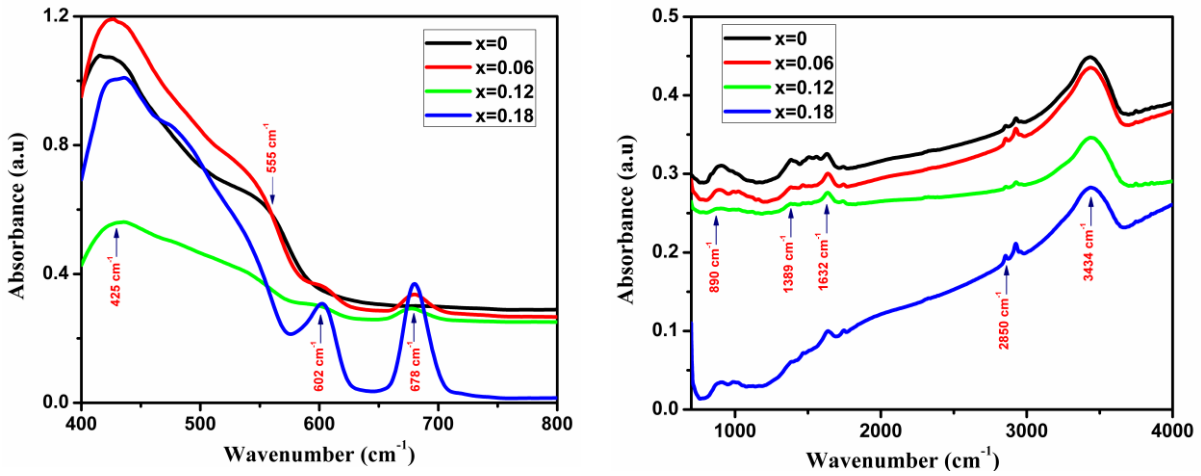

(a) **(b)**

Fig. 4.4. FTIR spectra of $Zn_{1-x}Co_xO$ series for **(a)** 400-800 cm^{-1} and **(b)** 700-4000 cm^{-1}.

4.3.4. UV-Visible spectra:

The UV-Visible optical absorption spectra of the $Zn_{1-x}Co_xO$ nanomaterials are displayed in figure 4.5 in the wavelength range 300-800 nm. The absorbance spectroscopy is projected to reflect on the coordination of the inserted ions in the host lattice, optical band gap, impurity concentration and oxygen vacancies etc. Two major peaks around 310 nm and 390 nm are explored in the absorption spectra. The peak at 310 nm is correlated to the band to band transition from valence to conduction band. The exciton peak of 390 nm of undoped ZnO gets shifted towards higher wavelength (395 nm) and the width of the peak increases with increasing cobalt concentration. This red shift is accredited to the decrease of energy gap. The *sp–d* exchange interactions with ZnO band electrons and *d* electrons of the cobalt ions lift up the oxygen 2*p* valence band and conduction band of zinc 4*s* [232]. The peak around 395 nm appears due to the defect states related to Zn and Co interstitials those lay below the conduction band. There are two mild anomalies around 568 nm, 659 nm and another significant peak at 605 nm have been explored belonging to the crystal field $d–d^*$ transitions of tetrahedrally coordinated Co^{2+} ions [233]. These peaks approve the replacement of zinc by cobalt ions placed in tetrahedral sites of ZnO wurtzite structure [232].

The small and comparatively broad intensity peak at about 490 nm is originated from the oxygen vacancy. Another detected peak at 690 nm in all the samples pure and doped is most likely have its origin in oxygen interstitials. The number of oxygen interstitials appears to increase with the increasing relatively smaller dopant ions [234] and the effect is visible through the increment in intensity of this peak.

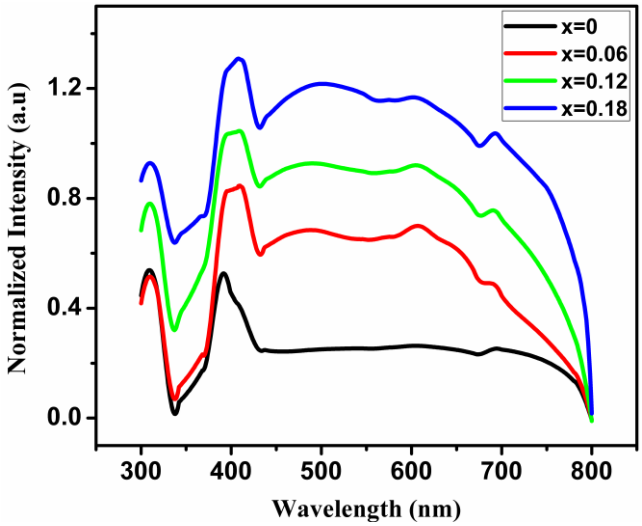

Fig. 4.5. Absorption spectra of $Zn_{1-x}Co_xO$ series.

4.3.5. Fluorescence spectra:

The room temperature fluorescence spectra of the $Zn_{1-x}Co_xO$ nanomaterials excited at 325 nm (Xe source) are presented in figure 4.6. The emission peak at 366 nm, 396 nm, 459 nm, 485 nm and 530 nm have been observed in the FL spectra of all the cobalt doped ZnO nanopowders. The ultraviolet peak at 366 nm (3.39 eV) is originated from recombination of exciton belonging to near band edge emission [207]. The peak around 396 nm (3.12 eV) corresponds to the radiative transition from unbiased donor level of Zn/Co interstitials, nearly 0.27 eV below the conduction band to the top of the valence band. Two blue emission peaks at 459 nm (2.7 eV) and 485 nm (2.56 eV) noticed for cobalt doped ZnO are most likely related to defect level. These emission peaks of blue region are originated from the electron transition from donor level of Zn/Co interstitial to acceptor level of neutral Zn/Co vacancy. The peak intensity decreases with increasing cobalt concentration because of concentration

quenching owing to cluster formation [235]. The peak around 530 nm is being elucidated by many researchers as the recombination of donor oxygen vacancy and acceptor zinc vacancy [236].

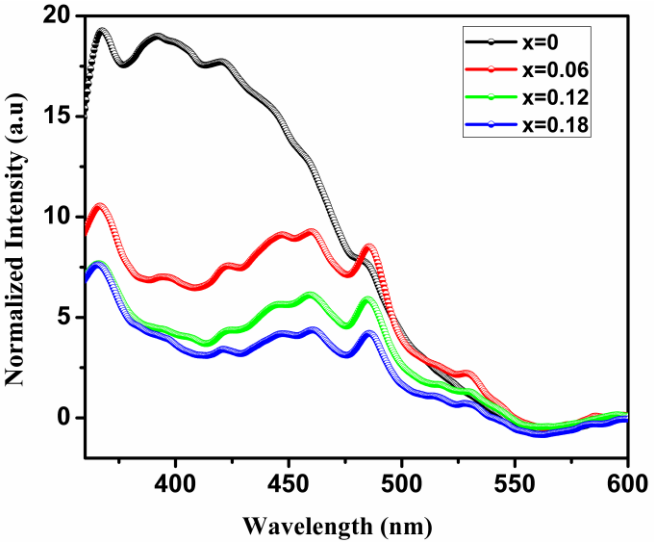

Fig. 4.6. FL spectra of $Zn_{1-x}Co_xO$ series.

4.3.6. Dielectric properties:

Awareness about the dielectric properties of cobalt doped ZnO nanomaterials is necessary for manipulating both the degrees of freedom of charge and spin for these nanocomposites in electromagnetic devices. Figure 4.7(a) depicts the room temperature dielectric dispersion in the frequency range of 100 Hz to 100 kHz. In these frequencies the dielectric constant is contributed by all the polarization mechanisms corresponds to electronic, ionic, dipolar and interfacial polarization. However, with increasing frequency some of the interfacial and dipolar modes cease because of inertia with respect to the field variation and in result the dielectric constant decreases. The graph indicates the presence of two different polarization mechanisms. At lower frequency the value of dielectric constant is large that seems to be originated according to Maxwell-Wagner mechanism. The grain boundary is expected to be highly insulating as compared to the less resistive grain interior. Conferring with this mechanism the grain interior capacitance is smaller than the grain boundary capacitance. The ratio of dielectric constant formed in these compounds due to the grain interior (bulk) and

grain boundary is of nearly 3 orders (~1000). Again, the dielectric constant of the synthesized $Zn_{1-x}Co_xO$ nanoparticles decreases with increase in concentration of cobalt ions. Further, the dielectric constant graph (figure 4.7(a)) reveals a peak at log[f(Hz)] = 3.65 i.e around 4.5 kHz for all the samples. The peak corresponds to the grain boundary relaxation for the sample with relaxation frequency of around 4.5 kHz. It is worth pointing here that the Maxwell-Wagner mechanism is dominant at high temperature and low frequency (< 10 kHz).

The dispersion curve of loss tangent is displayed in figure 4.7(b) and it exhibits low loss in the nanopowders. The loss tangent curve is involved with two contributions.

$$\tan\delta = \frac{\varepsilon''}{\varepsilon'} + \frac{\sigma_{dc}}{\omega\varepsilon'} \qquad (4.2)$$

The first term corresponds to the Debye type dipolar relaxation and the next term is attributed to dc conductivity. The Debye type relaxation is described by a Gaussian peak of the curve of loss tangent and the relaxation time (τ) obtained from the condition $\omega\tau = 1$, amounts to 2.65×10^{-5} s. The second term owing to conductivity is prevailed at low frequency and falls sharply with increasing frequency [219, 237].

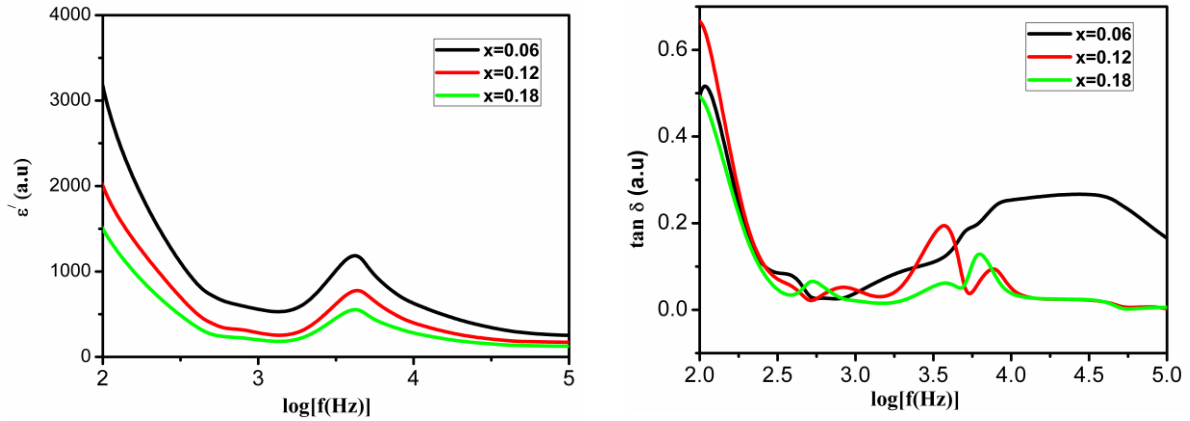

Fig. 4.7. Variation of **(a)** dielectric constant and **(b)** loss with frequency of Co-doped ZnO nanoparticles.

4.3.7. Magnetic property:

The variation of magnetization (M) with magnetic field (H) of $Zn_{0.94}Co_{0.06}O$ nanopowder has been recorded with applied field of ± 4 T at 5K by SQUID. Weak ferromagnetic nature of the compound at low temperature is exhibited in figure 4.8. The magnetic contribution in

the DMS is reported to originate from exchange interaction of *d–d* coupling of cobalt ions. The XRD analyses, FTIR, UV-Vis absorption and the FL spectra have confirmed the substitution of Co^{2+} ions at the Zn^{2+} sites of the wurtzite structure. However, Sundaresan et al. have reported that the ferromagnetism in the metal oxide nanoparticles, like CeO_2, Al_2O_3, ZnO etc. is due to the exchange interaction between localized spin moments created by the oxygen vacancies at the surface of nanoparticles [238]. The defect reconciled ferromagnetism of self-assembled ZnO and TM doped ZnO nanostructure was also explained by Barick et al. [128]. The role of oxygen vacancies in the development of ferromagnetism in cobalt doped ZnO nanoparticles was analyzed on the basis of noticeable change in the band structure of the host matrix on incorporation of cobalt [239]. Some reports also discussed the ferromagnetic behavior of cobalt doped ZnO nanopowders on the basis of bound magnetic polaron model. It is argued that the electrons locally trapped by oxygen vacancy on conquering an orbital overlapping with the *d* shells of cobalt neighbors create the BMP [120]. The existences of zinc interstitials and oxygen vacancies have been recognized through the UV-Vis absorption and FL spectra. With these experimental provisions the zinc interstitials and oxygen vacancies are believed as the key factors for the origin of ferromagnetism in the cobalt modified ZnO nanoparticles.

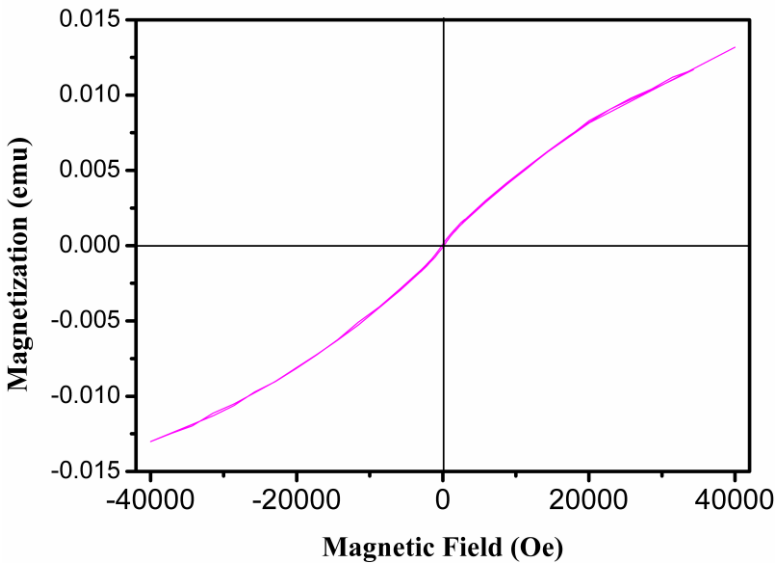

Fig. 4.8. M-H curve of $Zn_{0.94}Co_{0.06}O$ sample by SQUID.

4.3.8. Magnetoelectric coupling:

The magnetoelectric voltage coefficient varies with DC magnetic field for $Zn_{0.82}Co_{0.18}O$ sample at room temperature is exhibited in figure 4.9. The measured ME coupling effect in the sample is fundamentally generated by the coupling between magnetization and electric polarization in the bulk sample [240]. In case of single phase material, ME effect originates from the interaction between the sublattices of magnetic and ferroelectric phases, but the coupling between these phases is very weak and succeeds at lower temperatures [219]. The room temperature ferromagnetism is a consequence of the exchange interaction of $d-d$ coupling with cobalt ions. Such an interaction yields a shift of the Co^{2+} ion results in improper ferroelectric polarization and the perceived ME coupling effect. The sample was poled electrically and magnetically by which the dipole ordering proceeds and the sublattices effectively interact to produce the polarization for appropriate ME output [185]. The $Zn_{0.82}Co_{0.18}O$ pellet was positioned as discussed in sec. 2.2.8. The curve of figure 4.9 is a very good fit with second order polynomial. The ME voltage coefficient (α_E) [188, 189] without magnetic field according to the fitting plot is found to be 8.65 mV/(cm Oe). The second order (β) and third order (γ) coefficient are found to have values of 8.79×10^{-6} and -1.56×10^{-9} respectively in appropriate units.

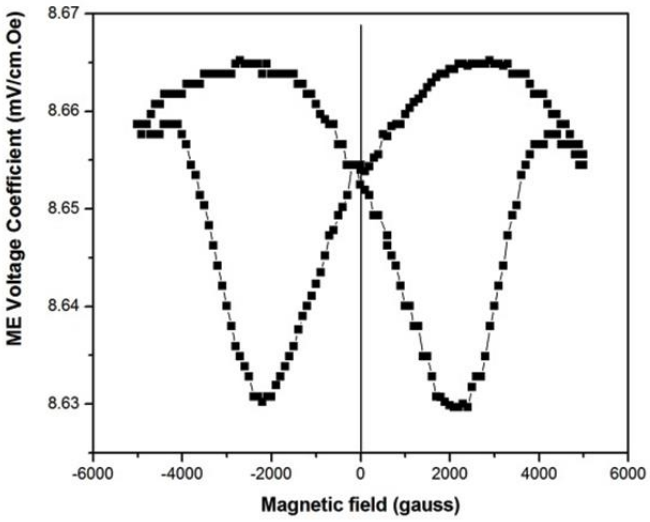

Fig. 4.9. Variation of ME voltage coefficient with DC magnetic field of $Zn_{0.82}Co_{0.18}O$ sample.

4.4. Conclusions:

The pure and doped ZnO nanoparticles have been synthesized by simple chemical precipitation technique at room temperature. The incorporation of cobalt has a great impact on the undoped ZnO, with regard to quality of crystallization and the orientation of crystallites. The average crystallite diameter of pure ZnO particles from TEM photograph is amounts to 30 nm. The particle size of the nanoparticles decreases with increasing concentration of cobalt ions. The intensity of absorption peaks of the doped materials at room temperature has been found higher than pure one and visible region emissions are present in the luminescence performance. These properties are accredited to the tune effect in the energy level of ZnO nanocompounds and also these materials can be useful for application in optoelectronic devices. The concentration of cobalt modifies the dielectric constant in host ZnO. All these materials exhibit low dielectric loss. SQUID study has explored weak ferromagnetic nature in cobalt doped ZnO nanomaterials. Though several origins have been accredited on account of magnetic behavior in the literature, in present work the zinc interstitials and oxygen vacancies originated from cobalt doping are believed to play the prime role for the ferromagnetic behavior. Materials with higher doping concentration perform as frustrated magnetic semiconductor. The coefficient of magnetoelectric coupling of the order of 8.65 mV/(cm Oe) in the compound with $x = 0.18$ is quite strong enough to exploit in electromagnetic coupling devices.

[Results of this work have been published in J. Mater. Sci.: Mater. Electron. 27 (2016) 12271-12278. (Ref. 233)]